

Behaviors of neutral and charged silicon self-interstitials during transient enhanced diffusion in silicon investigated by isotope superlattices

Yasuo Shimizu,^{1,a)} Masashi Uematsu,¹ Kohei M. Itoh,^{1,b)} Akio Takano,² Kentarou Sawano,³ and Yasuhiro Shiraki³

¹Department of Applied Physics and Physico-Informatics, Keio University, 3-14-1 Hiyoshi, Kohoku-ku, Yokohama 223-8522, Japan

²NTT Advanced Technology Corporation, 3-1 Morinosato Wakamiya, Atsugi 243-0124, Japan

³Research Center for Silicon Nano-Science, Advanced Research Laboratories, Musashi Institute of Technology, 8-15-1 Todoroki, Setagaya-ku, Tokyo 158-0082, Japan

(Received 27 August 2008; accepted 10 November 2008; published online 5 January 2009)

We investigated the contributions of neutral and charged silicon self-interstitials to self- and boron diffusion during transient enhanced diffusion in silicon. We simultaneously observed self- and boron diffusion in silicon using ^{nat}Si/²⁸Si isotope superlattices. A calculation based on diffusion equations involving {311} defects and boron-interstitial cluster models was employed to reproduce the diffusion profiles in silicon-implanted (intrinsic) and boron-implanted (extrinsic) silicon isotope superlattices, followed by annealing. To investigate the diffusion processes, the time evolution of the silicon self-interstitial profiles during the transient diffusion was simulated. The results directly demonstrate that excess neutral self-interstitials dominantly enhance the self-diffusion during the transient process in the intrinsic conditions, while doubly positively charged self-interstitials dominate the self-diffusion in the extrinsic conditions. © 2009 American Institute of Physics. [DOI: 10.1063/1.3054325]

I. INTRODUCTION

Boron (B) implantation and post-annealing processes are widely used for the formation of *p*-type shallow junctions in silicon (Si) electronic devices. For precise modeling of the behaviors of B during the formation processes, thorough understanding of the diffusion mechanisms involving the charge states of native point defects and transient enhanced diffusion (TED) is required. Regarding TED, {311} self-interstitial clusters produced by B implantation and annealing are the sources of supersaturated Si self-interstitials (*I*), which enhance B diffusion. In addition, B forms electrically inactive and immobile clusters even at concentrations far below the solubility limit under the supersaturation of *I* caused by ion implantation. TED of B in Si was extensively investigated by experiments¹⁻⁴ and the reliable modeling of B diffusion in Si involving TED and B clustering was published.⁵⁻⁷ Regarding the *I* contribution involving its charge states, first-principles calculations in the thermal-equilibrium conditions were reported recently.⁸ In such conditions, recent studies revealed the contributions of the neutral, singly, and doubly positive *I* (*I*⁰, *I*⁺, and *I*²⁺) and showed that *I*²⁺ dominates the self-diffusion in *p*-type doping conditions from simultaneous observations of dopants and Si using Si isotope multilayers.^{9,10} In order to develop the diffusion model involving *I* toward more precise process simulators, investigations of the behaviors of the charge states of *I* are required, especially in the initial diffusion process, where TED occurs and the diffusion takes place in non-equilibrium native defect conditions.

The present paper reports the contributions of neutral and charged *I* to self- and B diffusion during TED. Simultaneous observation of B and Si diffusion in Si isotope superlattices (SLs) was performed to know how B and Si atoms having the charge states interact. Based on the experimental diffusion profiles, we simulated the time evolution of *I*⁰, *I*⁺, and *I*²⁺ during TED in Si- or B-implanted Si isotope SLs. We show that the *I*²⁺ dominates the self-diffusion in B-implanted SLs, i.e., in the extrinsic conditions. In Si-implanted samples, i.e., without the Fermi level effect, *I*⁰ dominantly enhances the self-diffusion during the transient process.

II. EXPERIMENT

For both intrinsic and *p*-type conditions, a ^{nat}Si(10 nm)/²⁸Si(10 nm) isotope SL was grown by solid-source molecular beam epitaxy.¹¹⁻¹⁴ A high resistivity ($\rho > 2000 \Omega \text{ cm}$), 2 in., *n*-type, {001}-oriented floating zone ^{nat}Si (²⁸Si: 92.2%, ²⁹Si: 4.7%, and ³⁰Si: 3.1%) wafer was employed as a substrate. A ^{nat}Si buffer layer of ~100-nm-thick was grown prior to the growth of the isotope SL that is composed of the alternating layers of ^{nat}Si and isotopically pure ²⁸Si. For the intrinsic conditions, ²⁸Si⁺ ions were implanted at room temperature into the SL at an energy of 30 keV and a dose of $3 \times 10^{14} \text{ cm}^{-2}$. For simultaneous observation of B and Si, ¹¹B⁺ ions were implanted at 12 keV, $3 \times 10^{14} \text{ cm}^{-2}$. The SL wafer was cut into $5 \times 5 \text{ mm}^2$ squares for diffusion annealing at 850 °C (within $\pm 2 \text{ }^\circ\text{C}$) in a resistance furnace under a pure argon (99.99%) atmosphere. The depth profiles of ³⁰Si and ¹¹B were obtained by secondary ion mass spectrometry (SIMS).

^{a)}Electronic mail: yshimizu@appi.keio.ac.jp.

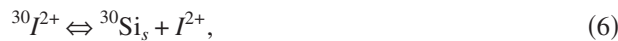
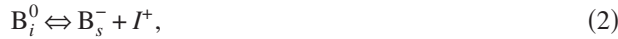
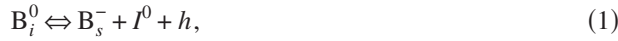
^{b)}Electronic mail: kitoh@appi.keio.ac.jp.

III. DIFFUSION MODEL

B diffusion in Si is primarily governed by the kick-out mechanism and B diffuses mainly via interstitial B or BI pairs rather than B vacancy (V) pairs.¹⁵ In addition, the V contribution to Si self-diffusion is negligibly small during TED because the I is supersaturated in over 10^4 .^{5,6} Therefore, we consider only the contribution of I in this study.

The B diffusion mechanism includes substitutional B (B_s^-), interstitial B (B_i), and I . Regarding the charge state of B_i , B isoconcentration diffusion experiments revealed that the B diffusivity is proportional to the B concentration,¹⁶ which shows that the charge difference between B_s^- and B_i is 1. Therefore, we consider only B_i^0 for the B diffusion. Regarding the charge states of I , B doping in Si increases the equilibrium concentration of positively charged I due to the Fermi level effect.^{9,10} In order to simulate the diffusion profiles, we basically used the diffusion model involving I^0 and I^+ as reported before.^{6,7,17} The recent studies of simultaneous observations of self- and dopant diffusion in Si showed that the I^{2+} contribution to self-diffusion is also important for p -type Si.^{9,10} Therefore, we introduced the contribution of I^{2+} and thereby the parameters were slightly changed, where more reliable values were extracted by the fitting of B interdiffusion profiles as has been done in Ref. 17.

The diffusion reactions involving B_s^- , B_i^0 , I^0 , I^+ , and I^{2+} can be described as



where h represents a hole. I^i and ${}^{30}I^i$ denote the I of ${}^{28}Si$ (matrix) and ${}^{30}Si$ with the charge states of i ($i=0, +1$, and $+2$), respectively. ${}^{30}Si_s$ represents a substitutional ${}^{30}Si$. These diffusion reactions, together with a kinetic equation to describe the time evolution of the self-interstitial cluster, allow the TED to be simulated by the following partial differential equations:

$$\frac{\partial C_{B_s}}{\partial t} = G_1 + G_2 + G_3 - G_8, \quad (7)$$

$$\frac{\partial C_{B_i}}{\partial t} = \frac{\partial}{\partial x} \left(D_{B_i} \frac{\partial C_{B_i}}{\partial x} \right) - G_1 - G_2 - G_3, \quad (8)$$

$$\frac{\partial C_{I^0}}{\partial t} = \frac{\partial}{\partial x} \left(D_{I^0} \frac{\partial C_{I^0}}{\partial x} \right) + G_1 - G_4 + G_5 - G_8, \quad (9)$$

$$\frac{\partial C_{I^+}}{\partial t} = \frac{\partial}{\partial x} \left(D_{I^+} \frac{\partial C_{I^+}}{\partial x} - D_{I^+} \frac{C_{I^+}}{p} \frac{\partial p}{\partial x} \right) + G_2 + G_6, \quad (10)$$

$$\frac{\partial C_{I^{2+}}}{\partial t} = \frac{\partial}{\partial x} \left(D_{I^{2+}} \frac{\partial C_{I^{2+}}}{\partial x} - 2D_{I^{2+}} \frac{C_{I^{2+}}}{p} \frac{\partial p}{\partial x} \right) + G_3 + G_7, \quad (11)$$

$$\frac{\partial C_c}{\partial t} = G_4, \quad (12)$$

$$\frac{\partial C^{30}Si_s}{\partial t} = G_5 + G_6 + G_7, \quad (13)$$

$$\frac{\partial C^{30}I^0}{\partial t} = \frac{\partial}{\partial x} \left(D^{30}I^0 \frac{\partial C^{30}I^0}{\partial x} \right) - G_5, \quad (14)$$

$$\frac{\partial C^{30}I^+}{\partial t} = \frac{\partial}{\partial x} \left(D^{30}I^+ \frac{\partial C^{30}I^+}{\partial x} - D^{30}I^+ \frac{C^{30}I^+}{p} \frac{\partial p}{\partial x} \right) - G_6, \quad (15)$$

$$\frac{\partial C^{30}I^{2+}}{\partial t} = \frac{\partial}{\partial x} \left(D^{30}I^{2+} \frac{\partial C^{30}I^{2+}}{\partial x} - 2D^{30}I^{2+} \frac{C^{30}I^{2+}}{p} \frac{\partial p}{\partial x} \right) - G_7, \quad (16)$$

$$\frac{\partial C_{B_{cl}}}{\partial t} = G_8, \quad (17)$$

where C_x ($x=B_s, B_i, {}^{30}Si_s, I^0, I^+, I^{2+}, {}^{30}I^0, {}^{30}I^+$, and ${}^{30}I^{2+}$) is the concentration of x and D_x is the diffusivity of x . C_c represents the concentration of I trapped in the clusters and $C_{B_{cl}}$ is the B concentration in the BI clusters. p represents the hole concentration. G_1 – G_8 represent the following generation terms:

$$G_1 = k_{1f}C_{B_i} - k_{1b}C_{B_s}C_{I^0}p, \quad (18)$$

$$G_2 = k_{2f}C_{B_i} - k_{2b}C_{B_s}C_{I^+}, \quad (19)$$

$$G_3 = k_{3f}C_{B_i}p - k_{3b}C_{B_s}C_{I^{2+}}, \quad (20)$$

$$G_4 = k_{4f}C_cC_{I^0} - k_{4b}C_c, \quad (21)$$

$$G_5 = k_{5f}C^{30}I^0 - k_{5b}C^{30}Si_sC_{I^0}, \quad (22)$$

$$G_6 = k_{6f}C^{30}I^+ - k_{6b}C^{30}Si_sC_{I^+}, \quad (23)$$

$$G_7 = k_{7f}C^{30}I^{2+} - k_{7b}C^{30}Si_sC_{I^{2+}}, \quad (24)$$

$$G_8 = -k_dC_{B_{cl}}, \quad (25)$$

where k_j ($j=1$ – 7) is the rate constant with f and b denoting forward and backward. For the initial profile of I in the $\{311\}$ clusters C_c , a “+1” model was used, where the implanted profiles are multiplied by a factor of 1.0.¹⁸ In order to describe TED, we used the following model of the time evolution of $\{311\}$ clusters during TED,⁶ which is involved in Eqs. (9) and (12). TED consists of two time regimes; the evolution is initially governed by Ostwald ripening of $\{311\}$ clusters and then by the dissolution of $\{311\}$ clusters. The essential parameters for the cluster evolution are the pseudo-equilibrium I concentration C_I^* , the time dependence rate for

cluster growth $k_{df} = -at + b$, and the dissolution rate k_{4b} . For the B clustering model, we used the analytical formula [Eq. (5) in Ref. 7] to estimate the initial profiles of clustered B, assuming that the B clusters are formed at the very early stages of annealing. For this simulation, we introduced k_d , which is defined as the rate constant of the dissolution of the B cluster involved in Eqs. (7), (9), and (17). The following parameter values at 850 °C were used for the simulation: $C_I^* = 1.8 \times 10^{14} \text{ cm}^{-3}$, $a = 5.5 \times 10^{-17} \text{ cm}^3 \text{ s}^{-2}$, $b = 2.3 \times 10^{-15} \text{ cm}^3 \text{ s}^{-1}$, $k_{4b} = 1.3 \times 10^{-2} \text{ s}^{-1}$, and $k_d = 6.7 \times 10^{-4} \text{ s}^{-1}$. Regarding the contribution of the charged I , $D_{I^0} C_{I^0}^{\text{eq}} / C_0 = 1.4 \times 10^{-19} \text{ cm}^2 \text{ s}^{-1}$, $D_{I^+} C_{I^+}^{\text{eq}} / C_0 = 2.6 \times 10^{-20} \text{ cm}^2 \text{ s}^{-1}$, and $D_{I^{2+}} C_{I^{2+}}^{\text{eq}} / C_0 = 2.7 \times 10^{-20} \text{ cm}^2 \text{ s}^{-1}$ were used, where C_0 represents the Si atom concentration, $5.0 \times 10^{22} \text{ cm}^{-3}$. These contributions of I^0 , I^+ , and I^{2+} are in good agreement with those reported before¹⁰ and the sum of them is consistent with the results of the total contribution of I to self-diffusion.¹⁹ In addition, for the total equilibrium concentration of I , we used the values from Ref. 19. We simulated the diffused B profiles using B diffusivity in thermal-equilibrium conditions.²⁰ To simulate the simultaneous diffusion of B and Si, Eqs. (7)–(17) were solved numerically by the partial differential equation solver ZOMBIE.²¹ In addition, we investigated the excess I in the intrinsic conditions using Si-implanted SLs. In this case, there are no diffusion reactions described in Eqs. (1)–(3). Therefore, G_1 – G_3 and G_8 should be considered as zero and Eqs. (9)–(16) were solved numerically.

IV. RESULTS AND DISCUSSION

A. I^0 contribution in the intrinsic conditions

In order to investigate the behavior of the excess I during TED without the Fermi level effect, we performed Si self-implantation into the $^{nat}\text{Si}/^{28}\text{Si}$ isotope SL. Figure 1 shows the depth profiles of ^{30}Si in the $^{28}\text{Si}^+$ -implanted (30 keV, $3 \times 10^{14} \text{ cm}^{-2}$) Si isotope SLs, followed by annealing at 850 °C for 1 and 4 h. The implanted ^{28}Si profiles were obtained by TRIM calculation.²² Here, ^{nat}Si layers have the natural abundance with 3.1% of ^{30}Si , whereas ^{28}Si layers are depleted of ^{30}Si . With such implantation condition, the periodic depth profile of ^{30}Si is almost unperturbed after the implantation in comparison with the profile of ^{30}Si before the implantation. Note that the actual interfaces between ^{nat}Si and ^{28}Si layers are abrupt (the degree of intermixing is only two atomic layers)^{13,14} and the smearing of the ^{nat}Si and ^{28}Si profiles is due to the SIMS artifact (knock-on mixing, etc.). This is the reason that the SIMS concentration of ^{30}Si in the ^{28}Si layer was above $\sim 10^{20} \text{ cm}^{-3}$ even in as-grown SLs as shown in Fig. 1, although the concentration of ^{30}Si in the enriched ^{28}Si layer was below 0.1%, which corresponds to the concentration of $5 \times 10^{19} \text{ cm}^{-3}$. In order to obtain the degree of the smearing, we introduced the mixing roughness information-depth (MRI) model that includes the parameters of atomic mixing and surface roughness for the theoretical description of the depth resolution function for SIMS profiles.²³ We extracted the parameter values by comparison with the isotopic profiles in the as-grown Si isotope SL by SIMS and a profile that initially has a rectangular shape us-

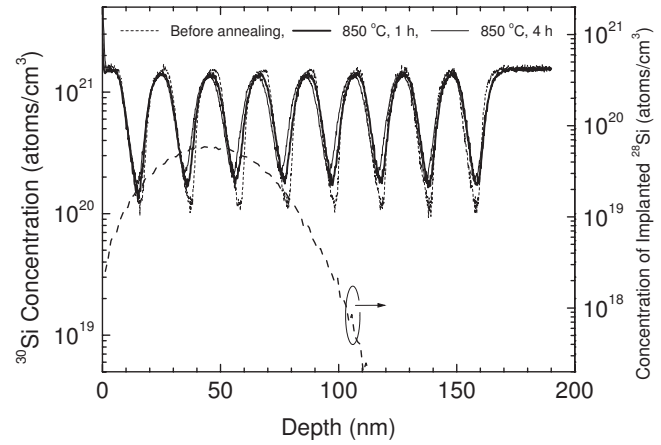


FIG. 1. SIMS depth profiles of ^{30}Si (upper profiles) in the $^{nat}\text{Si}/^{28}\text{Si}$ isotope SLs implanted with $^{28}\text{Si}^+$ at 30 keV, $3 \times 10^{14} \text{ cm}^{-2}$. The upper broken line and solid lines represent the experimental profiles of as-grown and after annealing at 850 °C for 1 and 4 h, respectively. The implanted $^{28}\text{Si}^+$ profile (lower profile) is calculated by TRIM.

ing the MRI model. Using the MRI parameters, we simulated the diffusion profiles by SIMS as follows: diffusion calculations were started with the rectangular profiles, and then, the MRI analysis was applied to the calculated diffusion profiles to compare with the SIMS profiles. In Fig. 1, the enhancement of Si self-diffusion is observed at the deeper region ($>40 \text{ nm}$) during the first 1 h annealing compared with that of the diffusion near the surface, which will be explained later.

We simulated the Si isotope profiles in Fig. 1 based on the diffusion models described in Sec. III and investigated the time evolution of I during this process. The simulated concentration profiles of I during 0–1 h annealing are drawn in Fig. 2. In the intrinsic conditions, the contribution of I^0 is larger than those of I^+ and I^{2+} . The I^0 concentration has a value of $C_I^* \sim 10^{14} \text{ cm}^{-3}$ at the initial stage ($t=1 \text{ s}$) with a flat profile in the bulk, whereas the value is going down to the C_I^{eq} toward the surface, which enhances the Si self-diffusion at the deeper region ($>40 \text{ nm}$) where the excess I is produced by the $^{28}\text{Si}^+$ self-implantation. Although such an I supersaturation gradient between the implanted region and the surface by the measurement using B marker layers was reported,^{24,25} the present work reports the direct observation of the enhanced Si self-diffusion using Si isotope SLs. We also observed the I supersaturation gradient for annealing at 800 °C (not shown in figures). At 60 s in Fig. 2, the excess I^0 is decreased to 10^{-3} compared with a value at 1 s. As diffusion annealing time increases, the I^0 concentration approaches C_I^{eq} . As shown in Fig. 1, a slower self-diffusion was observed between 1 and 4 h compared with that during 0–1 h, and our simulation shows that C_I is close to C_I^{eq} for longer annealing times, hence, the Si self-diffusion is in the thermal equilibrium. In conclusion, the excess I^0 mainly enhances the Si self-diffusion during TED at the initial stage in the area deeper than the implanted region.

B. I^+ contribution in the p -type conditions

In order to investigate the I behavior in the p -type conditions, we implanted $^{11}\text{B}^+$ ions into the Si isotope SL. Fig-

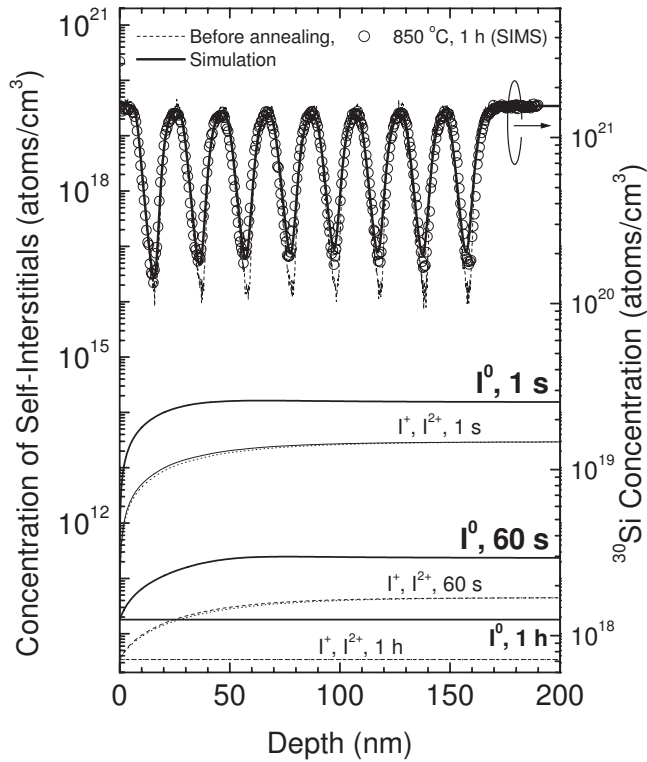


FIG. 2. Simulated self-interstitial (I^0 , I^+ , and I^{2+}) profiles (lower lines) in Si-implanted (30 keV , $3 \times 10^{14}\text{ cm}^{-2}$) Si isotope SLs during annealing at 850 °C for 1 s, 60 s, and 1 h. Upper broken line and open circles represent the SIMS profiles before and after annealing at 850 °C for 1 h, respectively. The upper solid curve represents the simulation result.

ure 3 shows the depth profiles of ^{30}Si and ^{11}B in the $^{nat}\text{Si}/^{28}\text{Si}$ isotope SLs implanted with B (12 keV , $3 \times 10^{14}\text{ cm}^{-2}$), followed by annealing at 850 °C for 1 h. Solid curves in Fig. 3 are simulation results that reproduce our experiments very well. While the depth oscillation of ^{30}Si is unperturbed before annealing, the annealing broadens its profile with much larger diffusivity than the thermal-equilibrium self-diffusivity of Si at 850 °C , which we have precisely determined using similar isotope SLs.²⁶ Furthermore, the ^{30}Si profile is especially broadened in the region 50–80 nm in depth, from which we quantitatively estimate the degree of excess I . Note that this depth region of 50–80 nm is away from approximately 40 nm, where the B concentration is the highest. Thus, the enhanced diffusion of ^{30}Si is not predominantly governed by the Fermi level effect. Although it has been shown that the excess I induces the anomalous diffusion of implanted B,^{2–4} this is the direct observation of the enhanced Si self-diffusion in a B-implanted Si.

In Fig. 4, the simulated concentration profiles of I at 850 °C for 5 s and 1 h are drawn with the corresponding B profiles. From the simulation, TED of B is observed within the 1 h annealing. Regarding the I concentrations during TED, I^{2+} dominates in the 0–70 nm region at the initial stage ($t < 5\text{ s}$), whereas I^0 is still higher in the region deeper than 70 nm from the surface. Our simulation reveals that the high concentration I^{2+} and I^0 broaden the ^{30}Si profile in the shallower and deeper region at the very initial stage, respectively. As annealing time increases, the excess I^0 , I^+ , and I^{2+} are

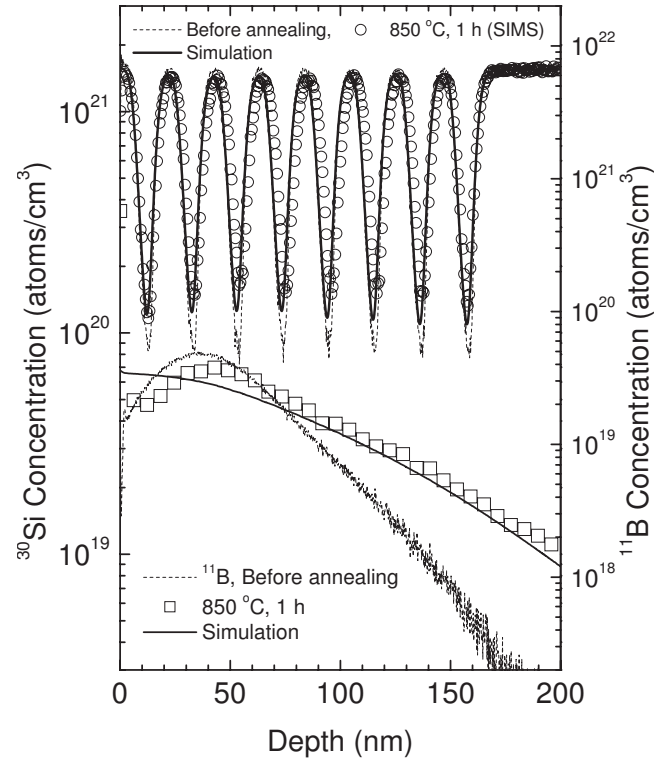


FIG. 3. SIMS and simulated depth profiles of ^{30}Si (upper profiles) and ^{11}B (lower profiles) in the $^{nat}\text{Si}/^{28}\text{Si}$ isotope SLs implanted with $^{11}\text{B}^+$ at 12 keV , $3 \times 10^{14}\text{ cm}^{-2}$. The upper profiles represent the Si profiles before (broken line) and after annealing at 850 °C for 1 h (open circles) and the lower profiles are the corresponding B profiles. Solid curves are the simulation results.

decreased compared with the values at 5 s. Then, the Fermi level effect becomes more remarkable with time because the B_s concentration increases by the dissolution of the B clusters. Therefore, the concentration of I^{2+} becomes relatively dominant especially near the surface, compared with those of I^0 and I^+ , that is, the I^{2+} dominantly enhances Si self-diffusion in the high concentration B region.

Furthermore, we simulated the profiles after 4 h annealing. Figures 5(a) and 5(b) show the depth profiles of ^{30}Si and ^{11}B after the annealing at 850 °C for 4 h, respectively. These SIMS profiles are well reproduced by the simulation using the same set of parameters as for 1 h. In Fig. 5(c), the simulated I profiles are shown, where I 's are almost in the thermal equilibrium. The Fermi level effect is still dominant for 1–4 h annealing, and TED was not observed for the annealing longer than 1 h because the excess I diffuses away from the B region into the Si bulk within 1 h of annealing. However, the concentrations of I are still above the equilibrium values even after 4 h. This is quite contrast to the I s in the Si-implanted samples, where the concentrations of I go down to the equilibrium states for 1 h as shown in Fig. 2. The I supersaturation in the B-implanted samples can be explained by the flux ratio between I and B_i . The supersaturation develops when $D_i C_i^{\text{eq}} / D_B C_B^{\text{eq}} < 1$, which indicates that I diffuses out slower than the B_i^0 diffuses in to become B_s^- .¹⁷ This flux balance generates an I supersaturation in the deep region^{9,10,17} as shown in Fig. 5(c).

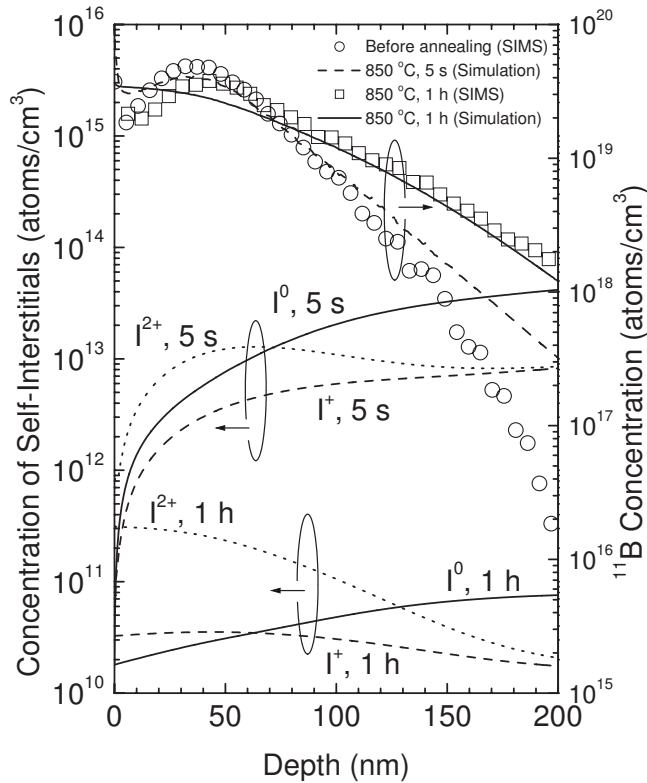


FIG. 4. Simulated self-interstitial (I^0 , I^+ , and I^{2+}) profiles (lower lines) in B-implanted (12 keV , $3 \times 10^{14} \text{ cm}^{-2}$) Si isotope SLs after annealing at $850 \text{ }^\circ\text{C}$ for 5 s and 1 h. The solid, broken, and dotted lines represent the profiles of I^0 , I^+ , and I^{2+} , respectively. In the upper region, the corresponding B profiles are shown.

V. SUMMARY

We presented the contribution of I to the self- and B diffusion in Si during TED. Simultaneous observation of the diffusion in Si- or B-implanted $\text{natSi}/^{28}\text{Si}$ isotope SLs was performed and the behaviors of neutral and charged I were investigated. A calculation based on the diffusion equations involving $\{311\}$ defects and BI cluster models was employed to reproduce the diffusion profiles of Si isotopes. We simulated the time evolution of the I profiles during the transient process to investigate the diffusion processes of Si isotopes in the ion-implanted SLs. The results directly demonstrate that excess I^0 dominantly enhances the self-diffusion during TED in the intrinsic conditions and that I^{2+} dominates the self-diffusion in the extrinsic conditions. This simultaneous observation of the self- and B diffusion in Si isotope SLs involving the time evolution of the I^0 , I^+ , and I^{2+} reveals the interactions between B and Si atoms during TED. The details of diffusion interactions between charged B and I into the next generation complementary metal-oxide semiconductor process simulators will be useful for the improvement of the simulation reliability.

ACKNOWLEDGMENTS

We acknowledge Y. Kawamura, M. Naganawa, and H. Oshikawa of Keio University and M. Nakamura, H. Ito, H. Ishikawa, and Y. Ohji of Selete for fruitful discussions. This work has been supported in part by the Grant-in-Aid for Scientific Research No. 205039, in part by the Research Pro-

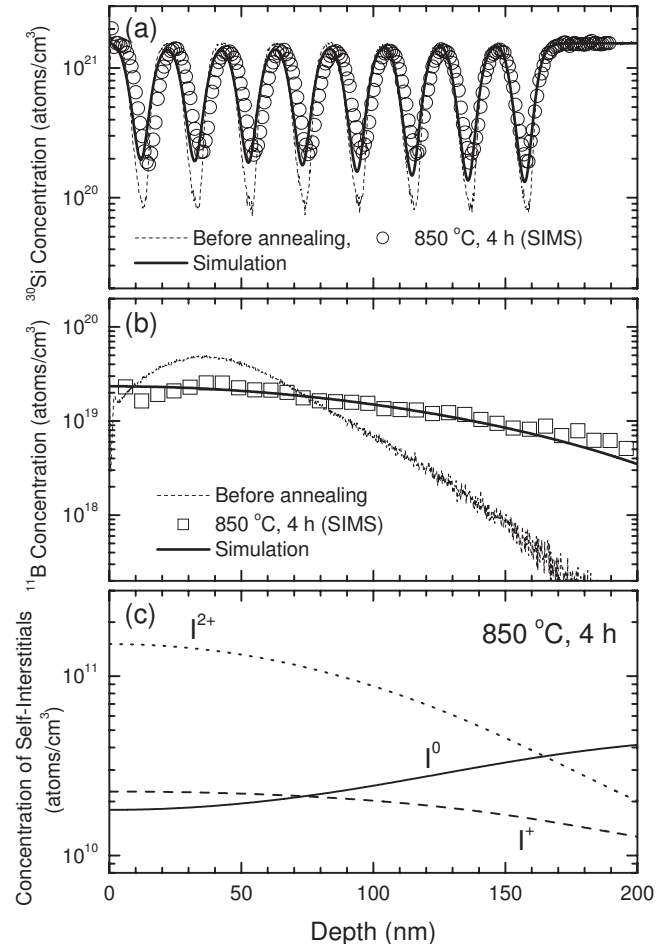


FIG. 5. (a) SIMS and simulated depth profiles of ^{30}Si in the $\text{natSi}/^{28}\text{Si}$ isotope SLs implanted with $^{11}\text{B}^+$ at 12 keV , $3 \times 10^{14} \text{ cm}^{-2}$. The broken line and open circles represent the SIMS profiles before and after annealing at $850 \text{ }^\circ\text{C}$ for 4 h, respectively. (b) The corresponding B profiles in the Si isotope SLs. (c) Simulated self-interstitial (I^0 , I^+ , and I^{2+}) profiles in the B-implanted Si isotope SLs after annealing at $850 \text{ }^\circ\text{C}$ for 4 h. The solid, broken, dotted lines represent the profiles of I^0 , I^+ , and I^{2+} , respectively.

gram on Collaborative Development of Innovative Seeds by JST, in part by the Special Coordination Funds for Promoting Science and Technology for INQIE, and in part by the Grant-in-Aid for the Global COE program “High-Level Global Cooperation for Leading-Edge Platform on Access Spaces (C12)” from MEXT.

¹C. S. Rafferty, G. H. Gilmer, M. Jaraiz, D. Eaglesham, and H.-J. Gossmann, *Appl. Phys. Lett.* **68**, 2395 (1996).

²N. E. B. Cowern, K. T. F. Janssen, and H. F. F. Jos, *J. Appl. Phys.* **68**, 6191 (1990).

³P. A. Stolk, H.-J. Gossmann, D. J. Eaglesham, D. C. Jacobson, C. S. Rafferty, G. H. Gilmer, M. Jaraiz, J. M. Poate, H. S. Luftman, and T. E. Haynes, *J. Appl. Phys.* **81**, 6031 (1997).

⁴S. C. Jain, W. Schoenmaker, R. Lindsay, P. A. Stolk, S. Decoutere, M. Willander, and H. E. Maes, *J. Appl. Phys.* **91**, 8919 (2002).

⁵M. Uematsu, *Jpn. J. Appl. Phys., Part 2* **36**, L982 (1997).

⁶M. Uematsu, *J. Appl. Phys.* **83**, 120 (1998).

⁷M. Uematsu, *J. Appl. Phys.* **84**, 4781 (1998).

⁸W. Windl, *Appl. Phys. Lett.* **92**, 202104 (2008).

⁹H. Bracht, *Phys. Rev. B* **75**, 035210 (2007).

¹⁰H. Bracht, H. H. Silvestri, I. D. Sharp, and E. E. Haller, *Phys. Rev. B* **75**, 035211 (2007).

¹¹K. Takyu, K. M. Itoh, K. Oka, N. Saito, and V. I. Ozhogin, *Jpn. J. Appl. Phys., Part 2* **38**, L1493 (1999).

¹²K. M. Itoh, J. Kato, M. Uemura, A. K. Kaliteevskii, O. N. Godisov, G. G.

- Devyatych, A. D. Bulanov, A. V. Gusev, I. D. Kovalev, P. G. Sennikov, H.-J. Pohl, N. V. Abrosimov, and H. Riemann, *Jpn. J. Appl. Phys., Part 1* **42**, 6248 (2003).
- ¹³T. Kojima, R. Nebashi, K. M. Itoh, and Y. Shiraki, *Appl. Phys. Lett.* **83**, 2318 (2003).
- ¹⁴Y. Shimizu and K. M. Itoh, *Thin Solid Films* **508**, 160 (2006).
- ¹⁵H.-J. Gossmann, T. E. Haynes, P. A. Stolk, D. C. Jacobson, G. H. Gilmer, J. M. Poate, H. S. Luftman, T. K. Mogi, and M. O. Thompson, *Appl. Phys. Lett.* **71**, 3862 (1997).
- ¹⁶M. Miyake, *J. Appl. Phys.* **57**, 1861 (1985).
- ¹⁷M. Uematsu, *J. Appl. Phys.* **82**, 2228 (1997).
- ¹⁸M. D. Giles, *J. Electrochem. Soc.* **138**, 1160 (1991).
- ¹⁹H. Bracht, N. A. Stolwijk, and H. Mehrer, *Phys. Rev. B* **52**, 16542 (1995).
- ²⁰M. Naganawa, Y. Kawamura, Y. Shimizu, M. Uematsu, K. M. Itoh, H. Ito, M. Nakamura, H. Ishikawa, and Y. Ohji, *Jpn. J. Appl. Phys.* **47**, 6205 (2008).
- ²¹W. Jüngling, P. Pichler, S. Selberherr, E. Guerrero, and H. W. Pötzl, *IEEE Trans. Electron Devices* **32**, 156 (1985).
- ²²J. F. Ziegler, J. P. Biersack, and U. Littmark, *The Stopping and Range of Ions in Matter* (Pergamon, New York, 1985).
- ²³S. Hofmann, *Surf. Interface Anal.* **21**, 673 (1994).
- ²⁴E. Lampin, F. Cristiano, Y. Lamrani, A. Claverie, B. Colombeau, and N. E. B. Cowern, *J. Appl. Phys.* **94**, 7520 (2003).
- ²⁵Y. Lamrani, F. Cristiano, B. Colombeau, E. Scheid, P. Calvo, H. Schäfer, and A. Claverie, *Nucl. Instrum. Methods Phys. Res. B* **216**, 281 (2004).
- ²⁶Y. Shimizu, M. Uematsu, and K. M. Itoh, *Phys. Rev. Lett.* **98**, 095901 (2007).